# Supporting Information

## Ureña et al. 10.1073/pnas.1401478111

### SI Materials and Methods

**Insects.** ***Blattella germanica.*** Specimens of *B. germanica* were obtained from a colony reared in the dark at 30 ± 1 °C and 60–70% relative humidity. All dissections and tissue sampling were carried out on carbon dioxide anesthetized specimens. Cockroaches undergo hemimetabolous development, where growth and maturation take place gradually and simultaneously during a series of nymphal instars. In particular, in our rearing conditions, *B. germanica* undergoes six nymphal instars (N1–N6) before molting into the adult. As *B. germanica* nymphs are miniature versions of the adults, the adult metamorphosis that takes place during the last nymphal instar (N6) is restricted to the transformation of the wing primordia into functional wings that spread just after the imaginal molt, to the acquisition of functional genitalia and to marked changes in cuticle pigmentation (Fig. S1). The classic example of adult morphogenesis in the hemimetabolous *B. germanica* is the transformation of the wing epithelium, which undergoes a dramatic cytoskeletal reorganization from a columnar epithelium of hexagonal cells to squamous flattened and stellate cells that interdigitate with the neighbor cells, thus allowing a fourfold expansion of the surface of the wing after the imaginal molt (Fig. S1 *C, D,* and *F–H*). Metamorphic changes include not only morphogenetic transformations but also cell death of tissues that are no longer required during the adult stage. Specifically, the prothoracic gland, the X-shaped tissue located in the prothorax that is responsible for the synthesis of ecdysteroids during nymphal stages, degenerates at the end of the last nymphal instar (Fig. S1 *I–L*).

***Tribolium castaneum.*** Wild-type *T. castaneum* strain and the enhancer-trap line *pu11* (obtained from Y. Tomoyasu, Miami University, Oxford, OH) were reared on organic wheat flour containing 5% (wt/wt) nutritional yeast and maintained at 29 °C in constant darkness. *pu11* is a transgenic line that has GFP expression in the wing and elytra imaginal discs of the larva and pupa as a result of an enhancer trap, as well as in the eye due to the presence of the 3XP3 artificial Pax6 element (1, 2). *T. castaneum* undergoes holometabolous development, which is characterized by marked changes between the larval and adult forms. The changes are so dramatic that an intermediate stage, the pupa, is required to accommodate the replacement of larval structures by adult ones (Fig. S6 *A–C*). In this regard, the specification of the holometabolan-specific pupal genetic program is controlled by the product of the *Broad-Complex* (*Br-C*) gene, whose expression is restricted to the transition between larval and pupal stages in *T. castaneum* (Fig. S6*D*). Under our rearing conditions, pupation takes place after seven larval instars (L1–L7) and lasts for 5 d. In contrast to hemimetabolous insects, metamorphosis in *T. castaneum* involves changes in the size, shape, and segmentation of all body appendages, as well as the occurrence of pupal-specific structures such as the gin traps and the typical microsculpture of the abdominal cuticle (Fig. S6 *E–K″*).

***Drosophila melanogaster.*** Flies were raised on standard *D. melanogaster* medium at 25 °C, unless otherwise required. Act-Gal4 (Actin-Gal4, a ubiquitous driver), Dll-Gal4 (Distal-less-Gal4, a distal appendage driver), UAS-GFP, UAS-dicer (used to enhance RNAi effectiveness), and Oregon R flies (OR-R, used as a wild-type control) were obtained from the Bloomington Stock Center. UAS-E93RNAi (KK108140) and UAS-E93RNAi (GD4449) are from the Vienna *Drosophila* RNAi Center (VDCR). The same phenotypes were obtained using both UAS-E93RNAi constructs. As in the case of *T. castaneum*, *D. melanogaster* undergoes holometabolan development, which includes the complete reorganization of most tissues during the prepupal and pupal stages.

**Cloning of *BgE93* cDNA.** We designed degenerate primers based on the sequence of the helix-turn-helix DNA binding domain of the Pipsqueak/E93 factor family. They were used to obtain the cDNA fragment of *BgE93* by means of RT-PCR. Total RNA was isolated using the GenElute Mammalian Total RNA kit (Sigma). PCR amplification was performed using, as a template, cDNA generated by reverse transcription from poly(A)+ RNA obtained from last nymphal instar prothoracic glands as previously described (3). The degenerate primers used for BgE93 amplification were as follows: forward (BgE93-F1), 5′-CCVAARMGDGGMAARTAYMG-3′ and reverse (BgE93-R1), 5′-TGHCKYTCYTTVACYTTGTA-3′. Amplification was carried out for five cycles at 94 °C for 30 s, 52 °C for 1 min, 72 °C for 1 min, and for 35 cycles of 94 °C for 30 s, 55 °C for 1 min, and 72 °C for 1 min. The 109-bp amplified fragment was subcloned into the pSTBlue-1 vector (Novagen) and sequenced. This procedure was followed by 5′-RACE (5′-RACE System, Version 2.0; Invitrogen) to obtain a longer sequence. For 5′-RACE, reverse primers were as follows: BgE93-R2, 5′-TGACCTTGTACTCGAGTGTGG-3′; BgE93-R3, 5′-TTGAACCGCTCTCACAGCTTCTAT-3′; BgE93-R5, 5′-CTCTGAACTTGTGGGAGTATC-3′; BgE93-R6, 5′-GCAACCAATGGTGGGGTGAACCT-3′; BgE93-R7, 5′-CTGTGGATCCACTGCTAGAAG-3′; BgE93-R8, 5′-GGACGGAATTTTCAGTATCACATT-3′.

As template, we used cDNA generated from last nymphal instar prothoracic glands. All PCR products obtained were subcloned into the pSTBlue-1 vector (Novagen) and sequenced in both directions. A final *BgE93* fragment of 886 bp was obtained (Fig. S2*B*).

**Quantitative Real-Time Reverse Transcriptase PCR.** Total RNA was isolated with the GenElute Mammalian Total RNA kit (Sigma). Each RNA preparation was DNase-treated (Promega) and reverse-transcribed with SuperScript II reverse transcriptase (Invitrogen) and random hexamers (Promega). Relative transcript levels were determined by real-time PCR (qPCR), using Power SYBR Green PCR Mastermix (Applied Biosystems). To standardize the qPCR inputs, a master mix that contained Power SYBR Green PCR Mastermix and forward and reverse primers was prepared (final concentration: 100 nM/qPCR). The qPCR experiments were conducted with the same quantity of organ equivalent input for all treatments, and each sample was run in duplicate using 2 μl of cDNA per reaction. All of the samples were analyzed on the iCycler iQ Real Time PCR Detection System (Bio-Rad). For each standard curve, one reference DNA sample was diluted serially. Primers sequences for qPCR analyses were as follows:

| *B. germanica* | |
|---|---|
| *BgE93* | E93-F2: 5′-CAAGCGGGGCAAATATCGCAATTA-3′ |
| | E93-R2: 5′-TGACCTTGTACTCGAGTGTGG-3′ |
| *BgActin5C* | BgActin5C-F: 5′-AGCTTCCTGATGGTCAGGTGA-3′ |
| | BgActin5C-R: 5′-TGTCGGCAATTCCAGGGTACATGGT-3′ |
| *BgBr-C* | BgBr-C-F: 5′-CTTAAAGCTCATAGAGTGGTGTTG-3′ |
| | BgBr-C-R: 5′-CACTTCACCATGGTATATGAATTC-3′ |
| *BgKr-h1* | BgKr-H1-F: 5′-ACAAATGTGGTGTATGCGCCAAGA-3′ |
| | BgKr-H1-R: 5′-GGTATGCACTTTGAGTTGTTTGGA-3′ |

| | |
|---|---|
| *T. castaneum* | |
| *TcE93* | Tc-E93-F: 5′-CTCTCGAAAACTCGGTTCTAAACA-3′ |
| | Tc-E93-R: 5′-TTTGGGTTTGGGTGCTGCCGAATT-3′ |
| *TcRpL32* | Tc-RpL32-F: 5′-CAGGCACCAGTCTGACCGTTATG-3′ |
| | Tc-RpL32-R: 5′-CATGTGCTTCGTTTTGGCATTGGA-3′ |
| *TcBr-C* | Tc-Br-C-F: 5′-TCGTTTCTCAAGACGGCTGAAGTG-3′ |
| | Tc-Br-C-R: 5′-CTCCACTAACTTCTCGGTGAAGCT-3′ |
| *TcKr-h1* | Tc-Kr-h1-F: 5′-AAGAAGAGCATGGAAGCACACATT-3′ |
| | Tc-Kr-h1-R: 5′-GAATCGTAGCTAAGAGGGTCTTGA-3′ |
| *TcCPR27* | Tc-CPR27-F: 5′-AGGTTACGGCCATCATCACTTGGA-3′ |
| | Tc-CPR27-R: 5′-ATTGGTGGTGGAAGTCATGGGTGT-3′ |
| *D. melanogaster* | |
| *DE93A* | DE93A-F: 5′-CACATCAGCAGCTATGAAATA-3′ |
| | DE93A-R: 5′-AACCGGCTATTGCTATGGGCTGTT-3′ |
| *DE93B* | DE93B-F: 5′-TCCACAGATATGCTGCATATTGTG-3′ |
| | DE93A-R: 5′-AACCGGCTATTGCTATGGGCTGTT-3′ |
| *DBr-C* | DBr-C-F: 5′-CATCTGGCTCAGATACAGAACCT-3′ |
| | DBr-C-R: 5′-CTTCAGCAGCTGGTTGTTGATGT-3′ |
| *DEdg78E* | DEdg78E-F: 5′-CCAATTCCCATCATCATGTACAAA-3′ |
| | DEdg78E-R: 5′-ATTGCTGGTCTCGTAGGCGTACT-3′ |
| *DAcp65A* | DAcp65A-F: 5′-CCGACAACGAATCCATATCCATTC-3′ |
| | DAcp65A-R: 5′-GGTATTTACAGGATCTCCTCGAAA-3′ |

**Quantification of Juvenile Hormone Levels.** Juvenile hormone (JH) titer was measured from haemolymph of *B. germanica* nymphs by liquid chromatography–mass spectrometry (LC-MS), using the method developed by ref. 4, with minor modifications to the protocol (5). For sample preparation, 70–80 μL of haemolymph from penultimate (N5) and last (N6) control and N6-*BgE93i* nymphs were extracted with a glass capillary and deposited into 300 μL 1:1 methanol:isooctane (vol/vol).

**RNA Interference.** ***B. germanica.*** RNAi in vivo in nymphs of *B. germanica* was performed as previously described (6, 7). To prepare the dsRNA targeted to *BgE93* (*dsBgE93*), a 318-bp fragment was subcloned into the pSTBlue-1 vector (Novagen). Similarly, a 294-bp fragment was selected to prepare a second dsRNA (*dsBgE93-2*) (Fig. S3*C*). Control dsRNA consisted of a noncoding sequence from the pSTBlue-1 vector (*dsControl*). Single-stranded sense and antisense RNAs were obtained by transcription in vitro, using either SP6 or T7 RNA polymerases from the respective plasmids, and resuspended in water. To obtain the dsRNAs, equimolar amounts of sense and antisense RNAs were mixed, heated at 90 °C for 5 min, cooled slowly to room temperature, and stored at −20 °C until use. Formation of dsRNA was confirmed by running 1 μL of the reaction products in 1% agarose gel. dsRNAs were suspended in diethyl pyrocarbonate-treated water and diluted in Ringer saline to a final concentration of 5–8 μg/μL, and 1 μL of the solution was injected into the abdomen of newly emerged penultimate (N5) or last (N6) instar nymphs, previously anesthetized on carbon dioxide. When the *dsBgE93* was injected into the abdomen of freshly ecdysed penultimate instar (N5) nymphs, *BgE93* mRNA levels in the wings, prothoracic glands, and epidermis decreased dramatically 6 d after the molt into the following N6 stage (Fig. S3 *D–F*). Specimens injected with *dsControl* were used as negative controls. The specificity of the phenotypes obtained with the injection of *dsBgE93* was confirmed by using the second *dsBgE93-2* dsRNA (Fig. S3*H*). The primers used to generate templates via PCR for transcription of the dsRNAs were as follows: dsBgE93-F, 5′-GAAACAGAACCTCCTTTCAAAAGG-3′; dsBgE93-R, 5′-AAAGTGTGAACCTGCCCGATGAA-3′; dsBgE93-2-F, 5′-CACAGTGCCCTAGGACCTTATGTT-3′; and dsBgE93-2-R, 5′-GGACGGAATTTTCAGTATCACATT-3′.

***T. castaneum.*** For RNAi in vivo in *T. castaneum*, a 348-bp *TcE93* fragment (*dsTcE93*) was subcloned into the pSTBlue-1 vector (Novagen). Then, the dsRNA was prepared as described for *B. germanica*. For the in vivo treatment, mid-last instar larvae (L7) of the *T. castaneum pu11* line were selected and anesthetized with ether for 3 min and then aligned on double-stick tape. *dsTcE93*, concentrated up to 4 μg/μL, was injected into the abdomen of these larvae, using a glass capillary needle connected to a syringe. Larvae were then kept at 29 °C until processed. Similarly to *B. germanica*, the dsRNA treatment resulted in a significant reduction of *TcE93* expression (Fig. S7*A*). The primers used to generate templates via PCR for transcription of the dsRNA were as follows: dsTcE93-F, 5′-AAATAACGGTGATACAGTGTCAAG-3′ and dsTcE93-R, 5′-TTGTAGTCCATCTCGGAGATGGAA-3′.

For the developmental expression analysis of *E93* in *B. germanica*, *T. castaneum*, and *D. melanogaster*, mRNAs were isolated from 5 to 10 animals per time point. All of the developmental mRNA profiles are representative of three independent replicates.

**Treatments with Methoprene in Vivo.** For juvenile hormone mimic treatment, mid-penultimate instar nymphs of *B. germanica* were topically treated on their dorsal side with increasing concentrations of methoprene (isopropyl (E,E)-(RS)-11-methoxy-3,7,11-trimethyldodeca-2,4-dienoate) per specimen in 1 μL of acetone. Controls received the same volume of solvent. At the desired stage, the nymphs were subjected to mRNA expression analysis.

**Microscopy, Histological Analysis, and Immunocytochemistry.** All dissections of *B. germanica* nymphal and adult tissues were carried out in Ringer's saline on carbon dioxide-anesthetized specimens. Prothoracic glands for DAPI staining were fixed in 4% paraformaldehyde and permeabilized in PBS-0.2% Tween (PBT) and then incubated for 10 min in 1μg/mL DAPI in PBT. Forewings and hindwings for rodamine-phalloidin staining were extracted from the wing pads and incubated in 300 ng/mL rodamine-phalloidin in PBT. After two washes with PBT, the tissues were mounted in Mowiol 4–88 (Calbiochem). *T. castaneum* and *D. melanogaster* dissections of legs, antennae, mandible, maxilla, hindwings, and forewings were also carried out in Ringer's saline and mounted directly in Glycerol 70%. For *D. melanogaster* immunohistochemistry, 30 h after puparium formation (APF) pupal wings were fixed in 4% paraformaldehyde in PBS for 30 min and then rinsed and treated with PBS containing 0.3% Triton X-100 for two consecutive washes of 20 min each. Wings were incubated with mouse anti-Broad-Complex (1:100 dilution; Developmental Studies Hybridoma Bank) in PBS containing 0.3% Triton X-100 and 1% BSA blocking agent for 1 h at room temperature. Antibody detection was carried out using Alexa Fluor 555-conjugated secondary antibodies (Molecular Probes). Stained wings were mounted in Vectashield (Vector Laboratories). All samples were examined with an AxioImager.Z1 (ApoTome 213 System; Zeiss) microscope, and images were subsequently processed using Adobe Photoshop.

**BrdU Labeling and Detection of Cell Death.** Proliferation of corpora allata cells from *B. germanica* was monitored by in vivo labeling with 5′-bromo-2-deoxyuridine (BrdU). Insects were injected with BrdU, and 12 h after injection, corpora allata were quickly dissected in saline and then fixed in Carnoy's fixative for 30 min, washed in PBS, and incubated in 70% methanol (MeOH) for 10 min, MeOH 30% hydrogen peroxide ($H_2O_2$) for 45 min, and 70% MeOH for 10 min. The tissue was washed in PBS and then incubated for 1 h in PBST-BSA. Tissues were incubated with 2 M HCl for 30 min to denature the DNA and allow access to the anti-BrdU antibody. The tissue was then washed 3 × 10 min in PBS and 2 × 10 min in PBST-BSA and placed in PBST-BSA-NSG blocking solution for 30 min. Mouse anti-BrdU was added at a 1:1,000 concentration to a PBST-BSA-NGT solution overnight at 4 °C. Next, the tissues were washed 3 × 10 min in PBST-BSA

and incubated 30 min in PBST-BSA-NSG before 2-h incubation with secondary antibody (1:100 in PBS-BSA-NSG). Finally, the tissues were washed 3 × 20 min in PBS, and immunoreactive cells were visualized by incubation in a solution of 3,3′-diaminobenezidine in PBS containing $H_2O_2$ and nickel chloride. To detect cell death in prothoracic glands, TUNEL assays were performed using the In Situ Cell Death Detection Kit, Fluorescein (Roche), following the manufacturer's instructions. Staged prothoracic glands were fixed in 4% paraformaldehyde in PBS for 30 min, washed in PBST (0.1% Triton-PBS), and permeabilized by incubation in 0.1% Sodium Citrate-0.1% Triton-PBS for 30 min. Samples were rinsed in PBS and incubated in TUNEL reaction mixture for 1 h at 37 °C. Finally, samples were mounted in Mowiol 4–88 (Calbiochem) and examined with an AxioImager.Z1 (ApoTome 213 System; Zeiss) microscope.

**Scanning Electron Microscopy.** Control and *TcE93i* pupae of *T. castaneum* were carefully taken out of the pupal cuticle with forceps, 5 d after pupation. Then, they were fixed in 80% ethanol and dehydrated with a series of graded ethanol solutions (90%, 95%, and 100%) for 15 min in each solution, critical-point dried using $CO_2$, sputter-coated with gold-palladium, and observed under a Hitachi S-3500N scanning electron microscope.


1. Lorenzen MD, et al. (2003) piggyBac-mediated germline transformation in the beetle Tribolium castaneum. *Insect Mol Biol* 12(5):433–440.
2. Tomoyasu Y, Denell RE (2004) Larval RNAi in Tribolium (Coleoptera) for analyzing adult development. *Dev Genes Evol* 214(11):575–578.
3. Maestro O, Cruz J, Pascual N, Martín D, Bellés X (2005) Differential expression of two RXR/ultraspiracle isoforms during the life cycle of the hemimetabolous insect Blattella germanica (Dictyoptera, Blattellidae). *Mol Cell Endocrinol* 238(1-2):27–37.
4. Westerlund SA, Hoffmann KH (2004) Rapid quantification of juvenile hormones and their metabolites in insect haemolymph by liquid chromatography-mass spectrometry (LC-MS). *Anal Bioanal Chem* 379(3):540–543.
5. Oostra V, et al. (2011) Translating environmental gradients into discontinuous reaction norms via hormone signalling in a polyphenic butterfly. *Proc Biol Sci* 278(1706): 789–797.
6. Cruz J, Martín D, Bellés X (2007) Redundant ecdysis regulatory functions of three nuclear receptor HR3 isoforms in the direct-developing insect Blattella germanica. *Mech Dev* 124(3):180–189.
7. Martín D, Maestro O, Cruz J, Mané-Padrós D, Bellés X (2006) RNAi studies reveal a conserved role for RXR in molting in the cockroach Blattella germanica. *J Insect Physiol* 52(4):410–416.

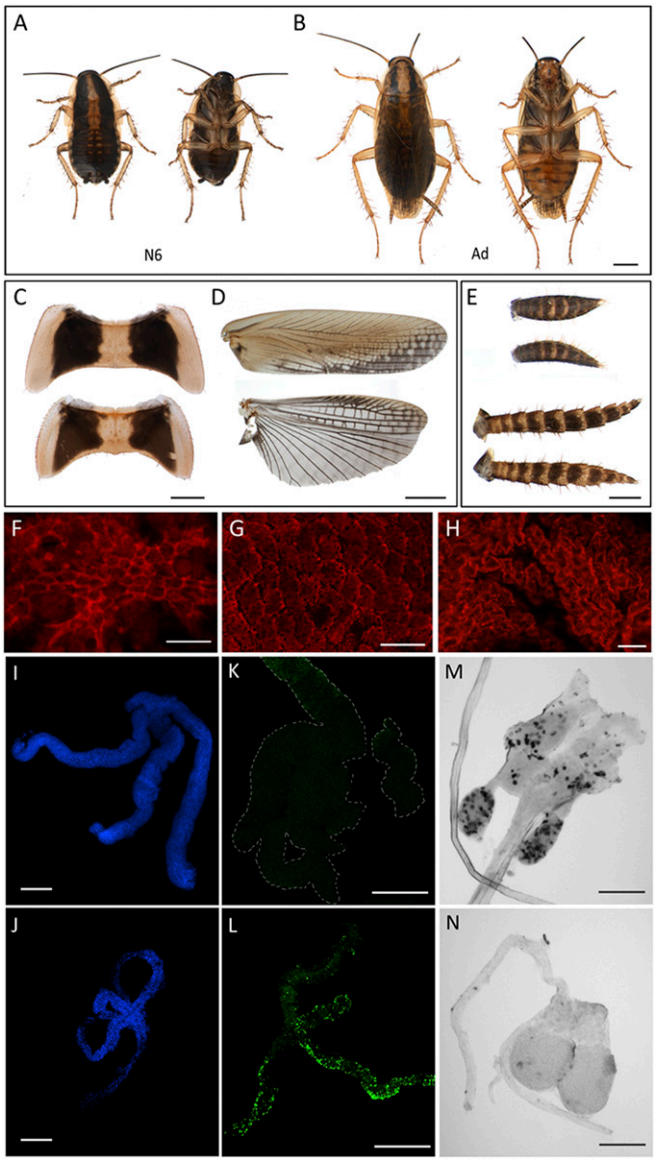


**Fig. S1.** Metamorphic changes in the hemimetabolous insect *B. germanica*. (*A* and *B*) Dorsal and ventral view of a last instar nymph (N6) characterized by the black cuticle and absence of functional wings (*A*) and a winged adult with brown cuticle and functional wings (*B*). (*C* and *D*) Wing pads of nymphal developing wings (*C*) and fully developed and extended adult wings (*D*). Forewings are in the upper part, and hindwings are in the lower part. (*E*) Nymphal (upper part) and adult (lower part) cercus. Note that the cuticular sculpturing and pigmentation differs greatly between nymph and adult. (*F–H*) Phalloidin-TRITC staining of the wing epithelium cell morphology of early (*F*), mid (*G*), and late (*H*) N6 nymphs. The morphogenetic transformation of the wing cells consists in the cytoskeletal reorganization from a columnar epithelium of hexagonal cells (*F*) to squamous, flattened, and stellate cells that interdigitate with the neighbor ones (*H*). This transformation allows a fourfold expansion of the wing surface after the imaginal molt. (*I–N*) Metamorphic changes in the prothoracic gland and corpora allata. (*I–L*) Prothoracic glands from a 7-d-old N6 nymph (*I* and *K*) and a 1-d-old adult (*J* and *L*) labeled with either DAPI (*I* and *J*) or TUNEL (*K* and *L*) to determine DNA fragmentation associated to cell death. Prothoracic gland degeneration takes place during the nymphal–adult transition, as revealed by TUNEL-positive nuclei in 1-d-old adult prothoracic gland, and correlates with the reduction in cell mass observed by DAPI staining. To improve TUNEL interpretation, the nymphal prothoracic gland is silhouetted. (*M* and *N*) BrdU labeling of the corpora allata of a 7-d-old N6 nymph (*M*) and a 1-d-old adult (*N*). corpora allata cells switch from a proliferative stage to an adult-specific nonproliferative phase. (Scale bars: *A, B*, and *D*, 2 mm; *C*, 1 mm; *E*, 0.5 mm; *F–H*, 10 μm; *I–N*, 100 μm.)

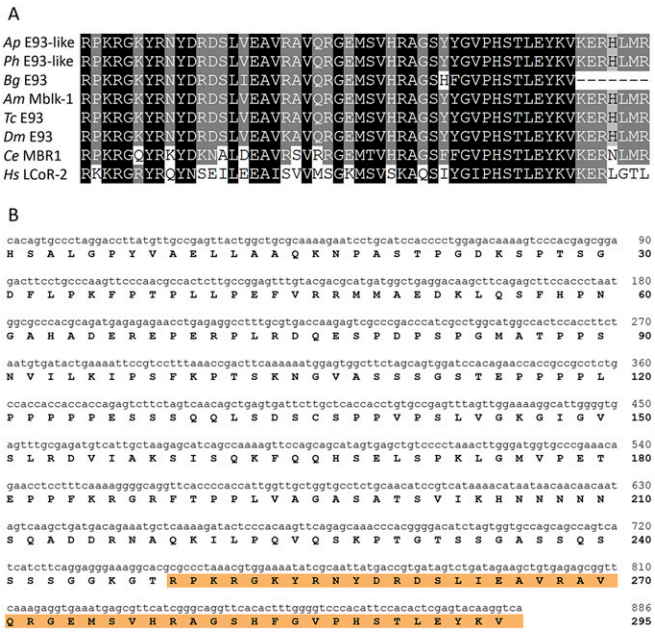


**Fig. S2.** (*A*) Comparison of the E93 Psq DNA-binding domain. *Acyrthosiphon pisum* (ApE93-like), *Pediculus humanus* (PhE93-like), *B. germanica* E93 (BgE93), *Apis mellifera* (AmMblk-1), *T. castaneum* (TcE93), *D. melanogaster* (DmE93), *Caenorhabditis elegans* (CeMBR1), and *Homo sapiens* (HsLCoR-2). Amino acid residues that are identical in all sequences are shaded black whereas identical residues present in at least 80% of the sequences are shaded gray. (*B*) Nucleotide and predicted amino acid sequences of *B. germanica* E93 (BgE93). The Pipsqueak (Psq) DNA-binding domain is highlighted.

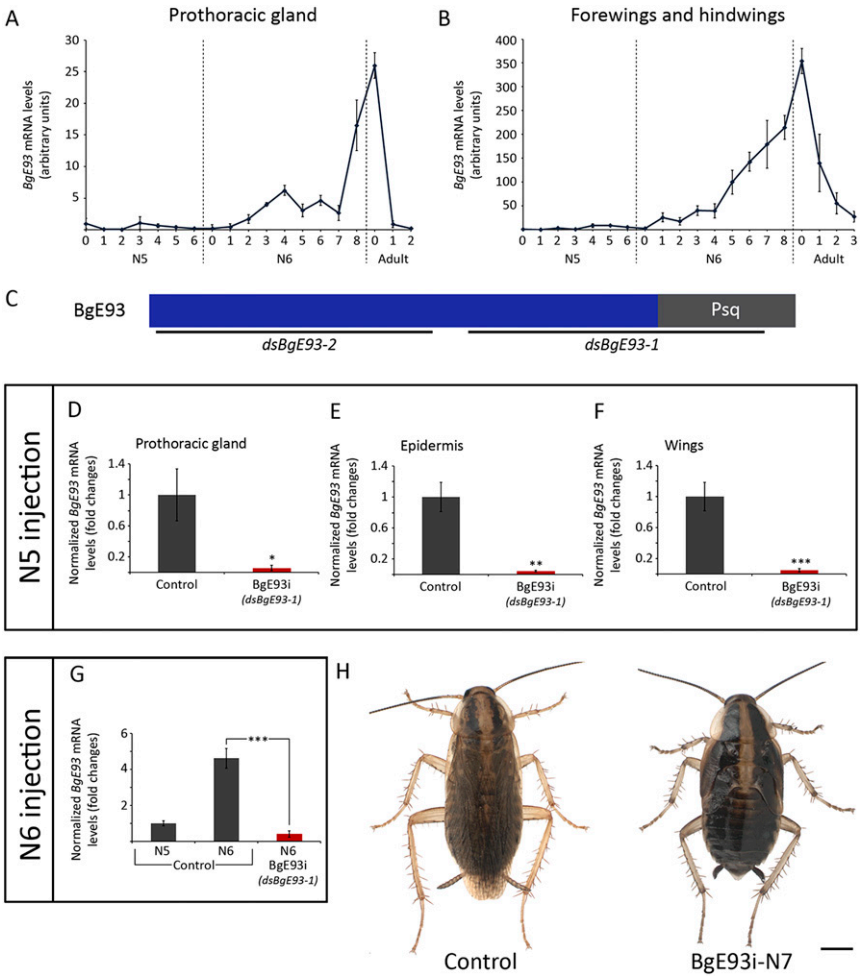


**Fig. S3.** (*A* and *B*) Developmental expression profile of *BgE93* in prothoracic glands (*A*) and wings (*B*) during the last two nymphal instars (N5 and N6) and the first days of the adult stage of *B. germanica* measured by qRT-PCR. Fold changes are relative to the expression of *BgE93* in 0-d-old N5 nymphs, arbitrarily set to 1. Error bars represent SEM ($n = 3$). (*C*–*F*) Effectiveness of *BgE93* RNAi in *B. germanica*. (*C*) Scheme of *BgE93* showing the regions used to generate the dsRNAs. (*D*–*F*) Effectiveness of *BgE93*-RNAi. A dose of 5 μg of *dsBgE93* was injected into newly emerged penultimate N5 nymphs (*BgE93i*), and *BgE93* mRNA levels in the prothoracic gland (*D*), epidermis (*E*), and wings (*F*) were measured 6 d after the molt into the following N6 stage by qRT-PCR. (*G*) Effectiveness of *BgE93*-RNAi carried out in N6 nymphs. The same dose of *dsBgE93* was injected into 1-d-old N6 nymphs to allow the disappearance of JH and *BgKr-h1*, and *BgE93* mRNA levels in wings were measured 3 d later by qRT-PCR. In all cases, equivalent experiments injecting a nonspecific *dsMock* (Control) served as negative control. Transcript abundance values for *BgE93* in *D*–*G* are normalized against *BgActin-5C* transcript. Fold changes are relative to the *BgE93* expression in control nymphs, arbitrarily set to 1. Vertical bars in *D*–*G* indicate the SEM ($n = 5$). (*H*) Confirming the specificity of the *BgE93* RNAi, newly-molted N5 nymphs treated with a second dsRNA (*dsBgE93-2*) show the same phenotype, as they molted into a supernumerary N7 nymph after two molts (*Right*). Asterisks indicate differences statistically significant as follows: $*P \leq 0.05$; $**P \leq 0.005$, and $***P \leq 0.001$ (*t* test). (Scale bar: 2 mm.)

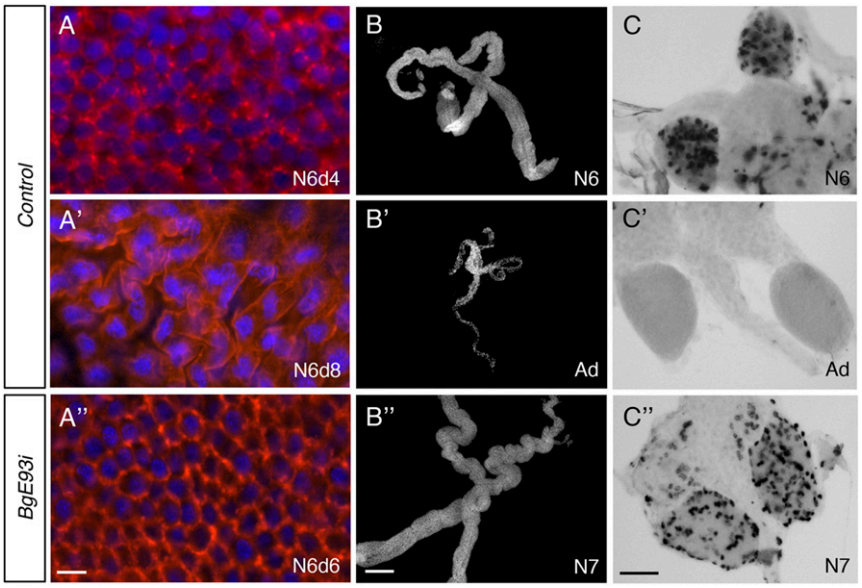


**Fig. S4.** All adult metamorphic transformations are blocked in *BgE93i* nymphs during N6. (*A*–*C*″) Newly emerged N5 nymphs were injected with *dsBgE93* (*BgE93i*) or with *dsMock* (Control), and metamorphic changes were analyzed after molting into the metamorphic N6 stage. (*A*–*A*″) Phalloidin-TRITC (red) and DAPI (blue) staining of (*A*) 4-d-old and (*A*′) 8-d-old wing of N6 control nymph and (*A*″) 6-d-old N6-*BgE93i* nymphs. (*B*–*B*″) DAPI staining of prothoracic glands of a (*B*) 5-d-old N6 control nymph and (*B*′) 5-d-old adult and (*B*″) a 5-d-old supernumerary *BgE93i* N7 nymph. (*C*–*C*″) BrdU labeling of the corpora allata of (*C*) a 3-d-old control nymph and (*C*′) 3-d-old adult and (*C*″) a 3-d-old supernumerary *BgE93i* N7 nymph. (Scale bars: *A*–*A*″, 20 μm; *B*–*B*″, 200 μm; *C*–*C*″, 50 μm.)

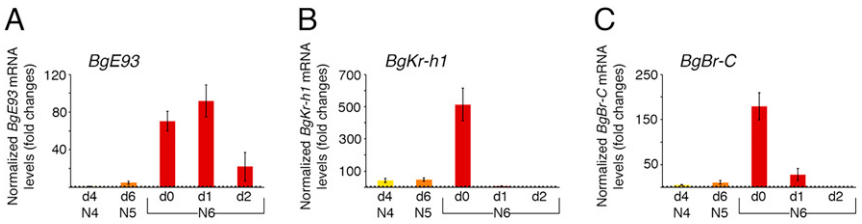


**Fig. S5.** *BgE93* up-regulation precedes the down-regulation of *BgKr-h1* and *BgBr-C* during the onset of the last nymphal stage of *B. germanica*. *BgE93, BgKr-h1 and BgBr-C* mRNA levels, normalized to *BgActin5C* (qRT-PCR), in the metamorphic wing tissue during N4 and the transition from the penultimate N5 to the final N6 nymphal instar. Fold changes are relative to the expression of *BgE93* in N4 nymphs, arbitrarily set to 1. Error bars represent SEM ($n$ = 3–4).

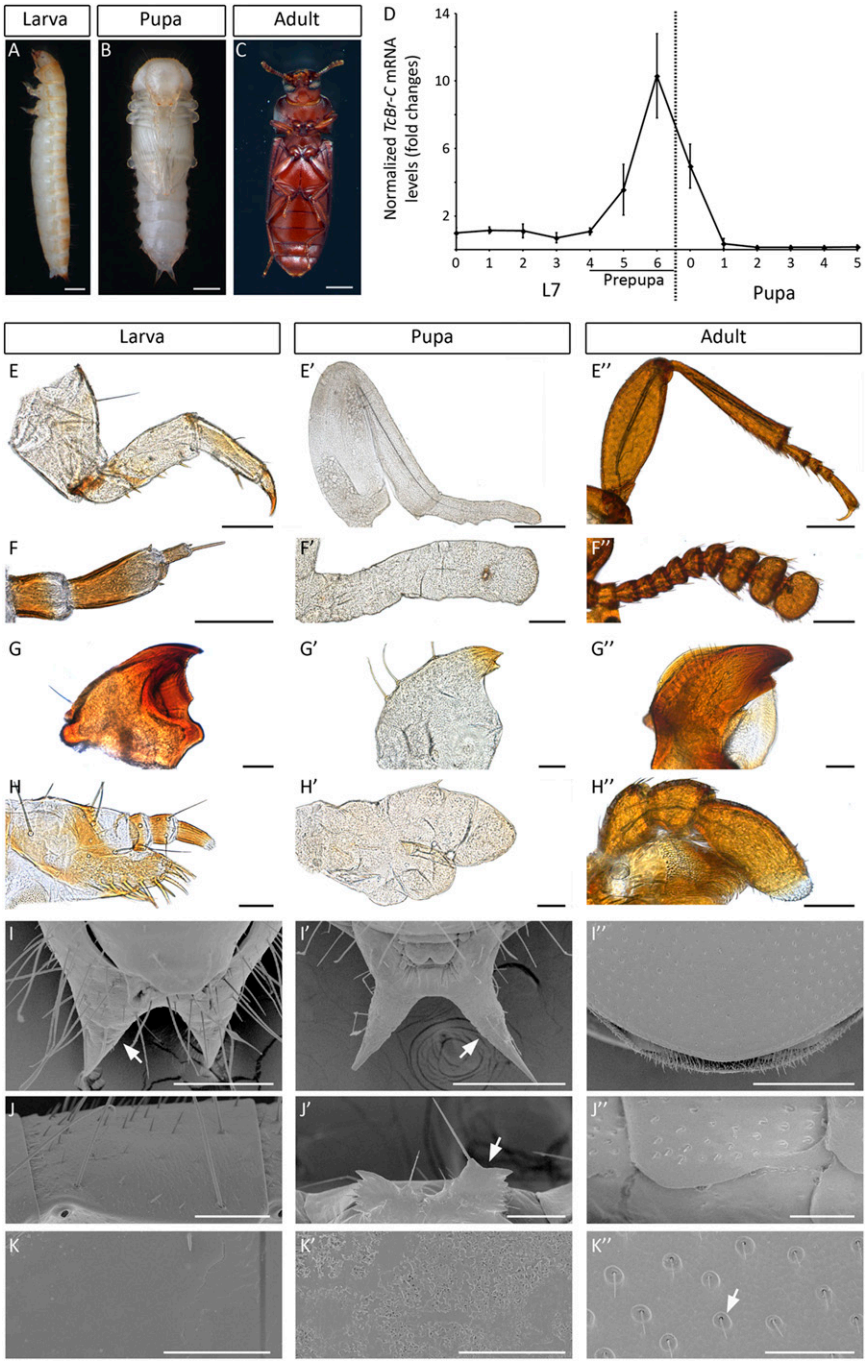


**Fig. S6.** Metamorphic changes in the holometabolous insect *T. castaneum*. In contrast to hemimetabolan development, metamorphosis in holometabolous insects involves a complex transformation from immature wingless larvae (*A*) to winged adults (*C*) by a transitory pupal stage (*B*). (*D*) Developmental expression profile of the pupal specifier *TcBr-C* relative to *TcRpL32* in the last larval stage (L7) and the pupal period (qRT-PCR). Fold changes are relative to *TcBr-C* expression in 0-d-old L7 larvae, arbitrarily set to 1. Error bars represent SEM ($n = 3$). (*E*–*K*″) Metamorphosis in *T. castaneum* involves changes in the size, shape, and segmentation of the body appendages. External morphology of different appendages from wild-type larva, pupa, and adult animals: hind leg (*E*–*E*″), antenna (*F*–*F*″), mandible (*G*–*G*″) and maxilla (*H*–*H*″). Metamorphic transformations also include changes in the urogomphi (*I*–*I*″), which are short in larvae (arrow in *I*), elongated and forked in the pupae (arrow in *I*′), and absent in adults (*I*″), as well as the appearance of pupal-specific structures such as gin traps (*J*–*J*″; arrows in *J*′) above pupal abdominal spiracles. Furthermore, the abdominal cuticle surface (*K*–*K*″) transforms from smooth in larvae (*K*) to a typical pupal microsculpture (*K*′) and to the adult cuticle with rounded pits with sensillae (arrows in *K*″). Scale bars: *A*–*C*, 0.5 mm; *E*, 100 μm; *E*′ and *E*″, 200 μm; *F*–*F*″, 100 μm; *G*–*H*″, 50 μm; *I* and *I*″, 200 μm; *I*′, 300 μm; *J*–*J*″, 100 μm; *K*–*K*″, 50 μm.)

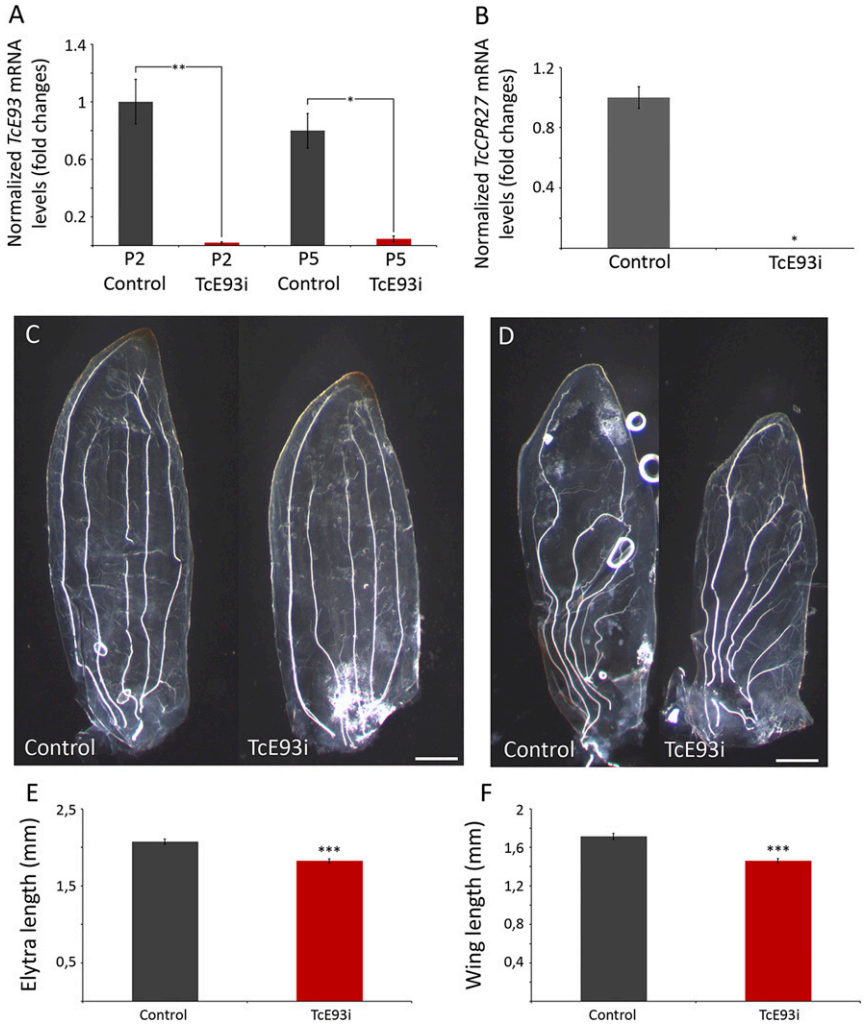


**Fig. S7.** Effectiveness of *TcE93* RNAi and the effect of *TcE93* depletion on the growth of elytra and wings in *T. castaneum*. (*A*) Effectiveness of *TcE93*-RNAi carried out in last instar larvae (L7). Mid-L7 larvae were injected with *dsTcE93* (*TcE93i*), and *TcE93* mRNA levels were measured 2 d and 5 d after pupation by qRT-PCR. Equivalent experiments injecting a nonspecific *dsMock* (Control) served as negative control. Transcript abundance values for *TcE93* are normalized against *TcRpL32* transcript. Fold changes are relative to the *TcE93* expression in 2-d-old control pupae, arbitrarily set to 1. (*B*) Effect of *TcE93*-RNAi on the expression of *TcCPR27,* an adult-specific cuticle gene used as an adult molecular marker, in 5-d-old pupae measured by qRT-PCR. In the absence of *TcE93*, the adult-specific *TcCPR27* gene is not induced. Vertical bars in *A* and *B* indicate the SEM (n = 3–5). Asterisks indicate differences statistically significant as follows: $*P \leq 0.05$; $**P \leq 0.005$ (*t* test). (*C*–*F*) TcE93 is required for proper growth of elytra and wings in *T. castaneum*. Elytra (*C*) and wings (*D*) from recently pupated control and *TcE93i* animals. (*E*) Length of elytra and (*F*) wings measured in mm, of control (black bars) and *TcE93i* pupae (red bars). Loss of *TcE93* produces a reduction of ~15% in elytra/wings length. Values represent the mean ± SEM ($n = 10$ for control, and $n = 9$ for *TcE93i*). Asterisks indicate differences statistically significant as follows: $***P \leq 0.00001$ (*t* test). (Scale bars: *C* and *D*, 0.2 mm.)

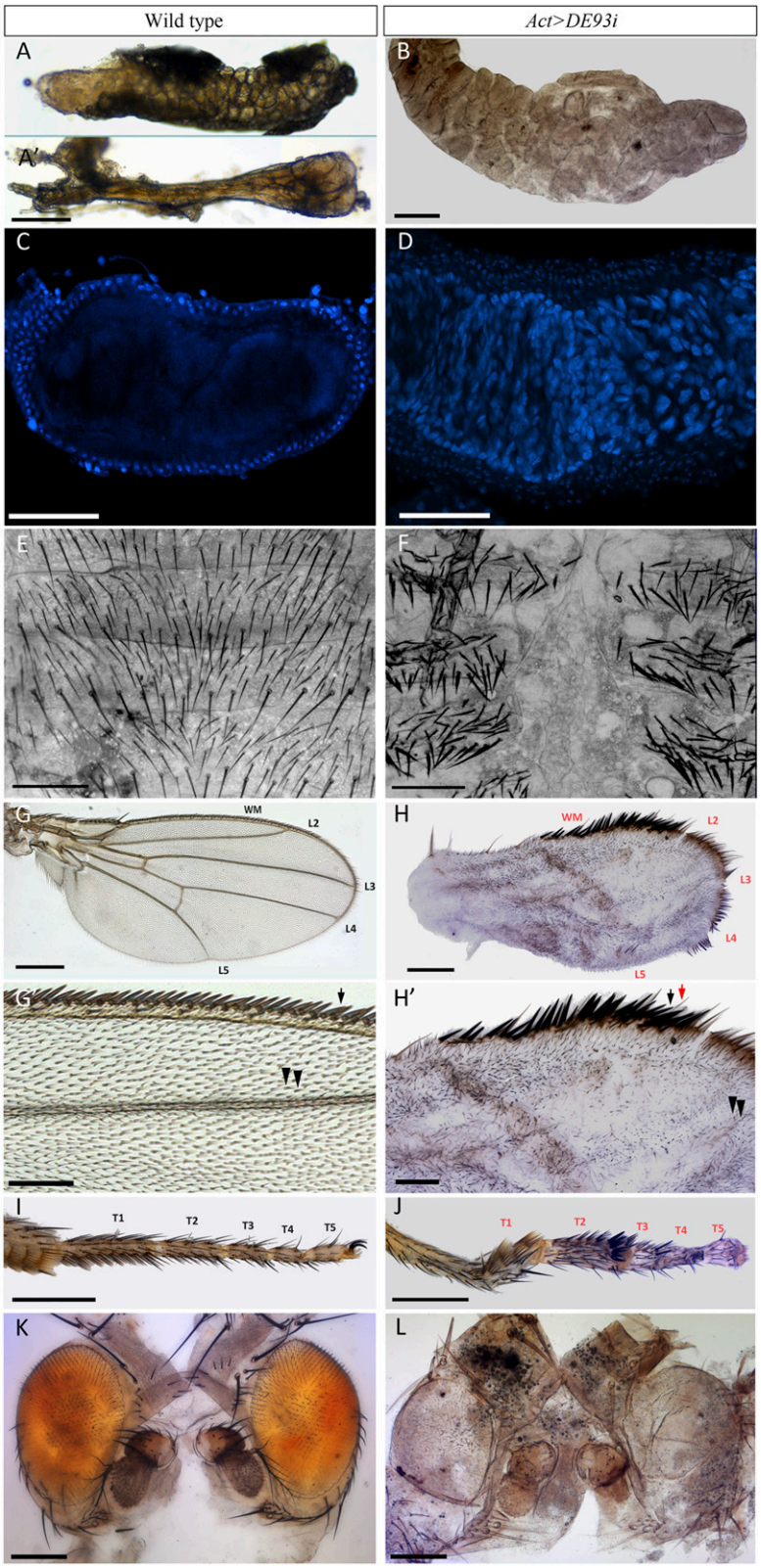


**Fig. S8.** Loss of *DE93* prevents metamorphosis in *D. melanogaster*. (*A–F*) Loss of *DE93* during the pupal stage impairs the degeneration of larval tissues during metamorphosis. (*A–B*) Staged salivary glands from 12 h (*A*) and 20 h (*A′*) APF wild-type and *Act>DE93i* (*B*) pupae. In the absence of *DE93*, salivary-gland cells fail to degenerate at 12 h APF. At 86 h APF, *Act>DE93i* salivary glands (*B*) have not reduced their cell mass as a result of cell death, compared with 20 h APF wild-type glands (*A′*). Instead, they still have the same size as wild-type glands before head eversion (12 h APF) (*A*). (*C* and *D*) Staged midguts stained with DAPI from (*C*) wild-type and (*D*) *Act>DE93i* animals at 86 h APF. In *Act>DE93i* midguts (*D*) larval enterocites fail to die and delaminate properly and get accumulated underneath the layer of adult enterocites, as revealed by the presence of DAPI-positive nuclei inside the midgut cavity. (*E*) Wild-type adult abdominal

Legend continued on following page

epidermis and (*F*) *Act>DE93i* animals. In the absence of *DE93*, the larval epidermal cells from the abdomen fail to die and delaminate, impairing the fusion of the histoblast nests and the proper differentiation of the adult abdomen. (*G–L*) Loss of *DE93* during the pupal stage prevents morphogenesis of adult structures. (*G*) Wild-type adult wings and (*H*) wings from *Act>DE93i* animals. In the absence of *DE93,* adult differentiation of the wing is blocked. Note that veins are mostly absent in wings from *Act>DE93i* animals compared with the wild type. (*G′*) High magnification of the anterior region of the wild-type and (*H′*) *Act>DE93i* wings showing disorganized and overlapping wing margin bristles (black and red arrows). *Act>DE93i* wing hairs (arrowheads) display polarity defects compared with the wild type. (*I*) Wild-type adult legs and (*J*) legs from *Act>DE93i* animals. In *Act>DE93i* legs, polarity, bristle specification, and tarsal segmentation are severely impaired. (*K*) Wild-type adult eyes and (*L*) eyes from *Act>DE93i* animals. Absence of *DE93* leads to smaller and unpigmented eyes. (Scale bars: *A* and *A′*, 500 μm; *G*, *I*, and *J*, 400 μm; *K* and *L*, 200 μm; *B*, *E*, *F*, *G′*, and *H*, 100 μm; *C*, *D*, and *H′*, 50 μm.)

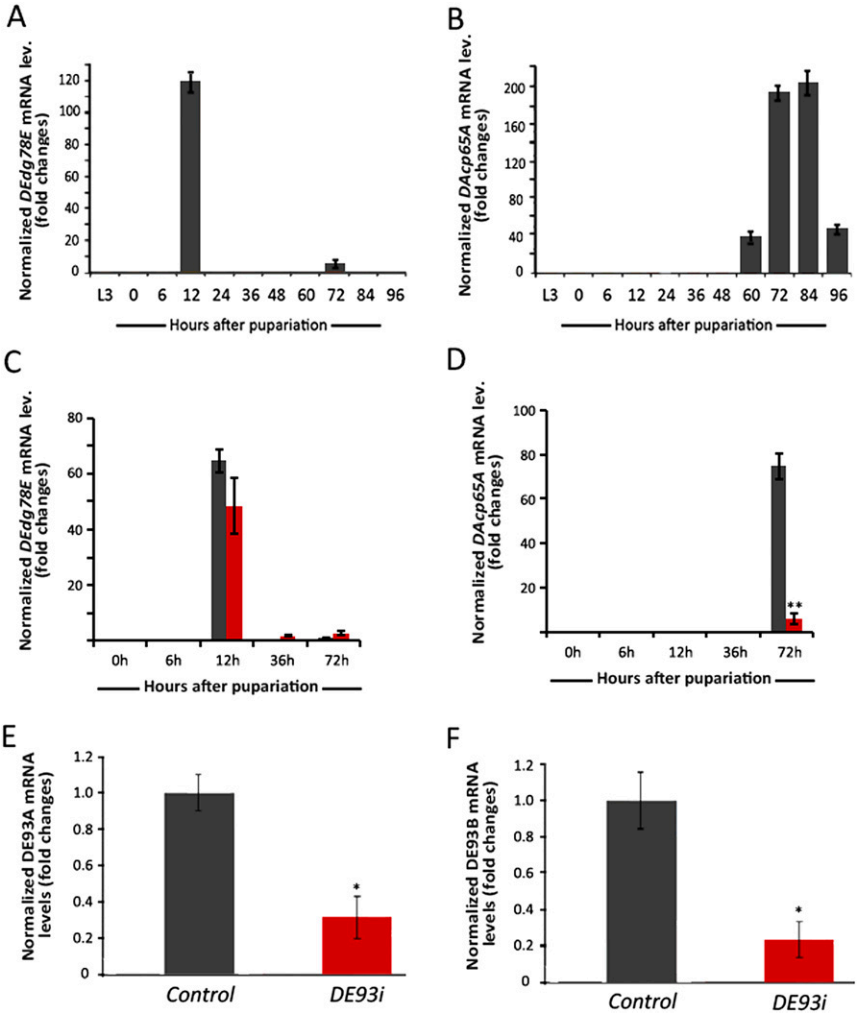


**Fig. S9.** Effect of *DE93* knockdown on expression of pupal and adult-specific genes during metamorphosis of *D. melanogaster* and effectiveness of *DE93* RNAi. (*A*) Developmental expression profile of the pupal-specific cuticle protein gene *DEdg78E* and (*B*) the adult-specific cuticle protein gene *DAcp65A*, measured by qRT-PCR relative to *DRpL32*, from mid-last larval stage (L3) to pupal stages. Error bars represent SEM ($n$ = 3–4). (*C*) Expression levels of *DEdg78E* and (*D*) *DAcp65A* measured by qRT-PCR relative to *DRpL32*, in wild-type (black bars) and *Act>DE93i* pupae (red bars). Whereas the expression of the pupal gene *DEdg78E* was not affected in *Act>DE93i* pupae, the induction of the adult-specific *DAcp65A* gene was completely impaired. (*E* and *F*) Effectiveness of *DE93* RNAi in *D. melanogaster*. (*E*) *DE93A* and (*F*) *DE93B* mRNA levels were measured by qRT-PCR at 12 h APF in wild-type (Control) and *Act>DE93i* pupae (*DE93i*). Transcript abundance values for *DE93A and DE93B* are normalized to *DRpL32* mRNA. Fold changes are relative to the expression of control pupae, arbitrarily set to 1. Error bars represent SEM ($n$ = 8–10). Asterisks indicate differences statistically significant as follows: $*P \leq 0.05$; $**P \leq 0.005$ ($t$ test).